inventions

MDPI

Article

Wide-Band Compact Substrate-Integrated Coaxial Line Transition

Mohamed Mamdouh M. Ali [1], Shoukry I. Shams [2,*], Mahmoud Elsaadany [3], Ghyslain Gagnon [3] and Abdelrazik Sebak [2]

[1] Department of Electrical Engineering, Faculty of Engineering, Assiut University, Assiut 71516, Egypt; mohamed.ali@ieee.org
[2] Department of Electrical and Computer Engineering, Concordia University, Montreal, QC H3G 1M8, Canada
[3] Department de Génie Électrique, École de Technologie Supérieure, Montreal, QC H3C 1K3, Canada
* Correspondence: shoukry.shams@ieee.org

Abstract

This article introduces a novel right-angle coax to Substrate Integrated Coaxial (SIC) transition, offering featured characteristics and performance in a compact size. An air-filled K-connector is used to ensure optimal transition in a compact form factor. The proposed transition covers the Ku-band up to 18 GHz, achieving a deep matching level below 20 dB. The transition is fabricated and tested in a back-to-back configuration, where it demonstrates impressive characteristics, including a matching level of −15 dB and an insertion loss of −0.22 dB/inch across the entire bandwidth for the back-to-back configuration.

Keywords: substrate integrated; coaxial transition; 6G applications; beamforming networks

1. Introduction

The evolution from 5G to 6G communication systems is pivotal, impacting the medical, food production, and defense sectors. The race for 6G standards has begun even before 5G is fully implemented worldwide. Both 5G and 6G use space diversity via MIMO and hybrid beamforming networks to enhance channel capacity, thereby accommodating more terminals and higher data rates per user [1,2]. These advancements promote the utilization of space diversity [3,4]. Space diversity is an essential tool for extending wireless network capability by directing the beam toward a specific user, enabling the use of the same frequency/time resources. This technology is challenging because available microwave components are still limited in both electrical performance and cost, making it difficult to adapt to this rapid expansion. Beamforming networks are the cornerstone of space diversity, consisting of multiple essential components such as couplers, dividers, antennas, and transitions. The required components must deliver outstanding performance in deep matching, wideband operation, and a very compact size. These characteristics can be achieved through both the innovative component design and the proper selection of the host guiding structure. Various guiding mechanisms have been proposed to support this future technological progression.

Different guiding structures are utilized to implement hybrid beamforming networks, such as microstrip lines [5], printed ridge gap waveguides [6,7], striplines [8–10], and Substrate Integrated Coaxial lines (SICL) [11]. Among all guiding structures, SICL configuration has superior characteristics, especially low dispersion and low radiation loss [12]. The low-loss characteristic ensures efficient power utilization, while the minimal dispersion eliminates the potential of signal distortion. In addition, this guiding mechanism is

Academic Editor: Ismail Fidan

Received: 10 February 2026
Revised: 12 March 2026
Accepted: 7 April 2026
Published: 9 April 2026

relatively compact and cost-effective. As a result, remarkable designs have been presented based on this technology with wide bandwidth and deep matching response [13,14]. However, the lack of superior transitions prevents widespread deployment of this technology.

The connection between the antenna feeding networks and the digital controller requires superior transitions that provide deep matching across the operating bandwidth. Moreover, the compact size significantly reduces the overall system cost. Hence, many articles have been published to propose transitions between SICL structures and other guiding mechanisms such as coplanar waveguides and rectangular waveguides [15–19]. Other articles have presented the transition to coaxial technology; however, they have not achieved full-band operation with deep matching characteristics [20–25]. A closer examination of prior SICL-based transitions reveals additional limitations. Vertical SICL-coaxial configurations achieve matching below −15 dB over 12–18 GHz but require metallic housings that complicate integration. Shielded suspended SICL designs exhibit reasonable matching but involve meticulous assembly and increased manufacturing complexity. Cascaded transmission line approaches offer deeper matching over narrow bandwidths but are lengthy and challenging to integrate. Other reported solutions, including rectangular waveguide transitions, broadband SICL-to-waveguide designs, and conductor-backed coplanar waveguide transitions, often suffer from relatively high insertion loss or rely solely on simulations without experimental validation [26–29]. These limitations highlight the need for a compact, wideband, low-loss transition that is practical for real-world systems. In addition, the aforementioned published design techniques are mostly based on direct connections terminated with open or short circuits, which have severe limitations in practicality and fabrication feasibility. This limitation will be discussed in detail in the coming section. This leaves room for improvement in proposing transitions that provide featured characteristics over full-band operation.

Here, we present an innovative solution for a right-angle SIC compact transition design. The motivation for this design stems from the need to overcome the limitations of prior SICL and waveguide transitions, which often exhibit high insertion loss, limited bandwidth, bulky metallic housings, or complex multilayer structures. The introduced transition covers the entire Ku-band while achieving a remarkable matching level exceeding 20 dB and low insertion loss, all without requiring metallic housings or complex multilayer structures. In addition to its wideband and low-loss performance, the proposed design demonstrates robust tolerance to fabrication variations, simplified integration into existing systems, and compatibility with compact beamforming networks. By combining these features, the proposed transition provides a practical and high-performance solution for integrated antenna feeding networks, addressing both performance and integration challenges observed in previous works. In the following sections, a detailed description of the design methodology adopted in this work will be provided, along with a critical assessment of the limitations of the direct connection.

2. Materials and Methods

2.1. Proposed SICL Design

The proposed SICL structure is shown in Figure 1, where the proposed SICL structure consists of a conductor sandwiched between two parallel ground planes printed on a dielectric substrate. The design and analysis of the proposed SICL structure involve careful consideration to ensure optimal performance of the proposed wideband transition. The width of the SICL and the dielectric substrate properties are selected to achieve single-mode operation within the desired frequency range. In the proposed design, a symmetrical SICL configuration is selected, where a Roger 6002 substrate with dielectric constant $\varepsilon_r = 2.94$ and loss tangent $\tan\delta = 0.0012$ is deployed for its low-loss properties and high-frequency

performance, enabling efficient signal propagation. In addition, platted vias are placed around the feed line, which offers an effective technique for suppressing higher-order mode propagation and reducing radiation by eliminating electromagnetic emissions. The proposed SICL parameters w_f, h_1, and h_2 for the line width, top substrate height, and bottom substrate height, respectively. These dimensions achieve an impedance of 50 Ω, where the dispersion relation of the proposed structure shown in Figure 1 shows the operation of the proposed SICL and allocates the higher-order mode outside the operating band beyond 20 GHz. All full-wave electromagnetic simulations were performed using CST Studio Suite 2025 [30] on a standard desktop PC equipped with an Intel Core i7 processor, 32 GB RAM, and Windows 11.

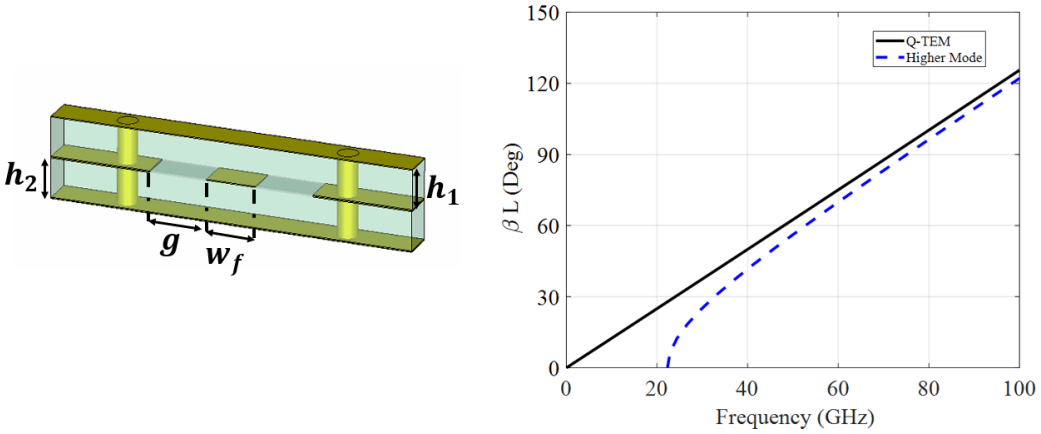

Figure 1. The geometrical configuration and simulated dispersion diagram of the proposed SICL structure.

2.2. Direct Transition Limitations

The straightforward design of the transition will be constructed through the direct connection of the coaxial inner conductor and the feed line center conductor. The signal can be guided in the desired direction by placing an open circuit at $\lambda/2$ or a short circuit at $\lambda/4$ or $3\lambda/4$. This configuration will be limited by the effectiveness of either the short or open circuits at the entire bandwidth, which is a critical aspect in wideband operation. Both configurations were implemented and simulated, where Figure 2a represents the structure's top view. In contrast, Figure 2 shows the response with a parametric sweep on the distance l_s. The parameter l_s represents the distance between the coaxial connector center point and the short/open circuit. Figure 2b highlights that the short circuit has a deeper matching level, as the open circuit cannot be realized perfectly with SICL technology. It can be depicted from both curves that both techniques can provide limited bandwidth as λ is defined at the band center and deviates at band edges.

Moreover, the substrate hole around the inner conductor represents a critical dimension with a tight tolerance. Any minor deviation in this dimension deteriorates the matching level significantly, as shown in Figure 2b, where the matching level reaches -5 dB. This highlights the sensitivity of this transition design to fabrication tolerances. The above-mentioned limitations highlight the motivation for exploring alternative solutions that feature wideband short- and open-circuit implementations with lower sensitivity.

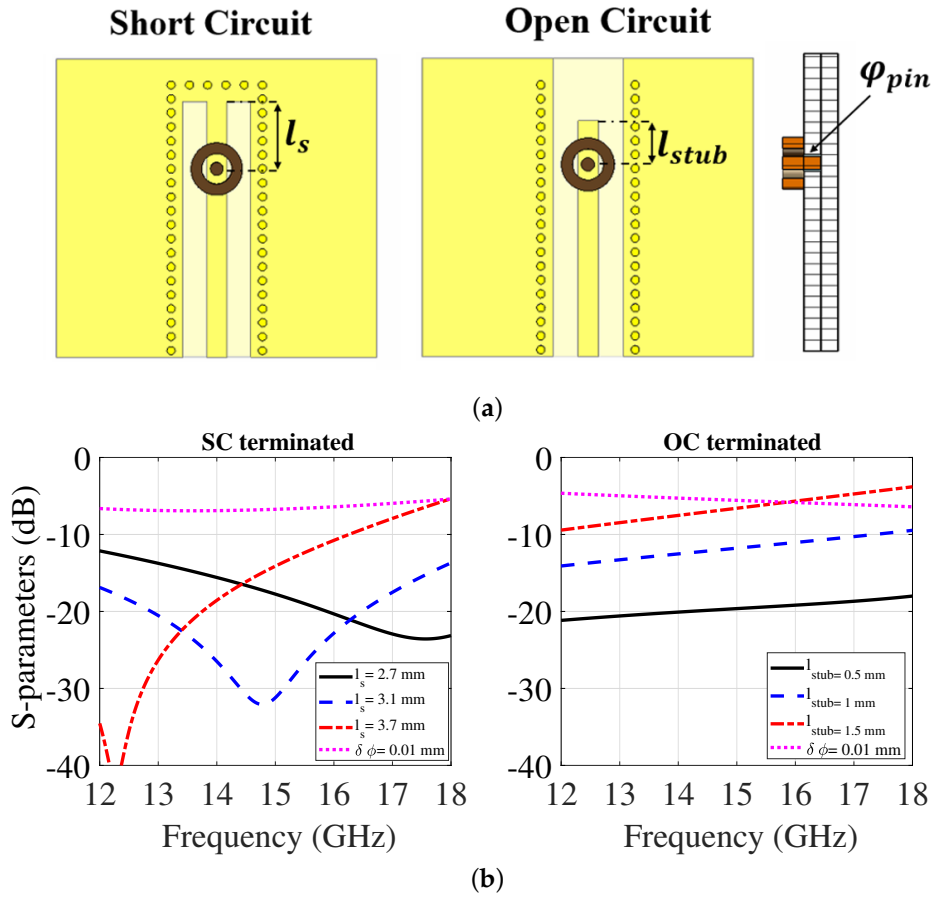

Figure 2. Direct transition from coaxial line to SICL based on open circuit and short circuit terminated. (**a**) 2-D configuration. (**b**) Simulated S-parameters.

2.3. Proposed Wideband Transition

The proposed wideband transition, illustrated in Figure 3a, overcomes the limitations of prior designs by incorporating innovative structural elements that enhance impedance matching, reduce reflections, and provide high-performance operation across a broad frequency spectrum. To overcome challenges posed by fabrication tolerances and ensure optimal signal integrity, the transition design incorporates several key features. Initially, a plated hole is created in the bottom-layer substrate with a diameter matching the coaxial line's outer conductor. This arrangement facilitates a smooth transition as the inner conductor of the coaxial line extends through this plated hole, as shown in Figure 3b. This configuration ensures the connection and maintains stable signal transmission. We proposed another tuning element in the form of a tuning pill with a diameter ϕ_{pill} attached to the inner conductor's pin. This pill ensures contact between the inner conductor and the top-layer ground, thereby minimizing reflections and improving overall performance. Furthermore, the core of the proposed design features a wideband short circuit positioned at the back of the SICL, incorporating a trapezoid-shaped conductor. Unlike a traditional rectangular short-circuit limited by narrow-band resonance, the tapered profile of the trapezoid facilitates a frequency-dependent reflection point. This mechanism ensures that the reflected wave maintains a near 180° phase shift relative to the incident parasitic reflections across the entire Ku-band. By leveraging this trapezoidal geometry, the transition achieves continuous destructive interference of unwanted reflections, ensuring superior impedance matching. To validate this physical mechanism, a parametric sweep of the back-short length (l_s) was conducted, as illustrated in Figure 4. The results demonstrate that l_s is the primary factor in controlling the phase cancellation. At the optimized length of 2.9 mm ,

the inductive reactance of the stub perfectly offsets the capacitive parasites of the junction, resulting in a return loss better than 20 dB from 12 to 18 GHz. Conversely, as l_s increases toward 4.3 mm, the physical distance approaches a half-wavelength ($\lambda_g/2$) at higher frequencies. This shifts the phase shift away from the 180° cancellation condition toward a constructive interference state, effectively shorting the transition point and leading to the total mismatch observed near 16.5 GHz.

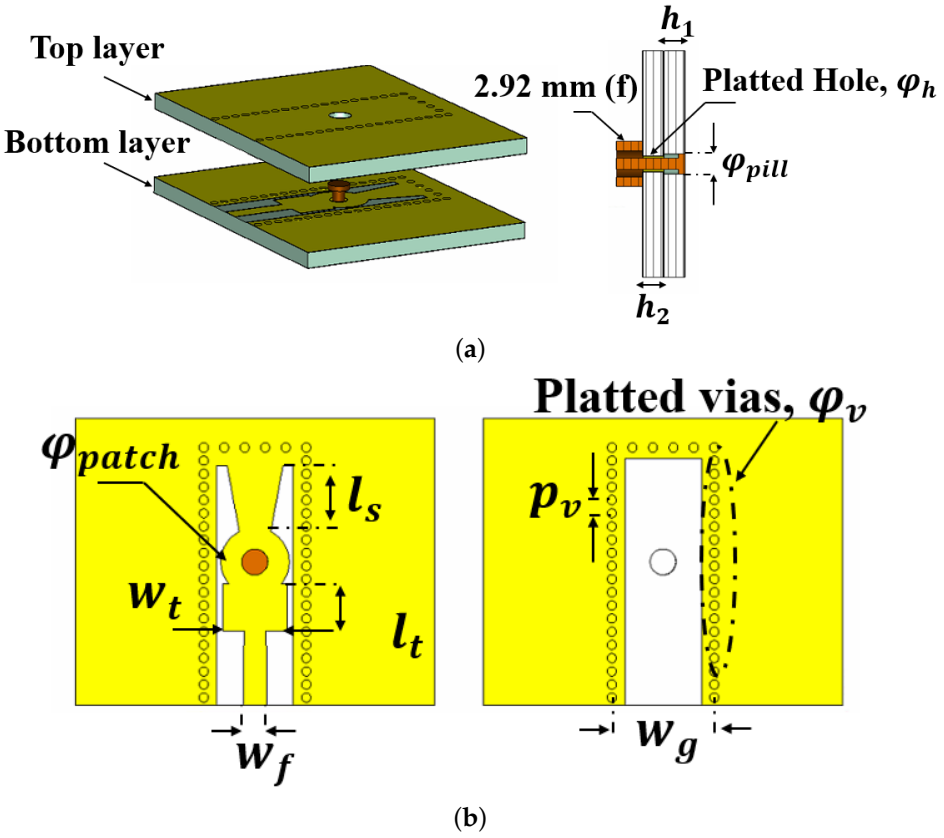

Figure 3. The geometrical configuration of the proposed SICL-to-coaxial line transition. (**a**) 3-D view. (**b**) Top-view.

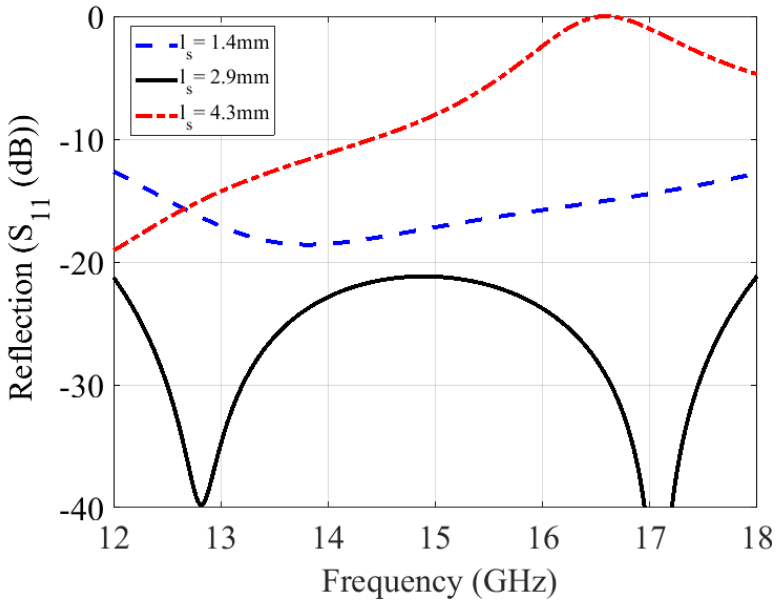

Figure 4. Simulated S_{11} of the proposed transition for various back-short lengths.

In addition to the trapezoid-shaped conductor and tuning pill, a circular patch is positioned at the connection point between the coaxial line and the SICL. This patch serves as a critical impedance-matching element that bridges the transition between the vertical coaxial pin and the horizontal SICL. As illustrated in the parametric sweep of the patch diameter (ϕ_{patch}) in Figure 5, this element dictates the positioning and depth of the transition's dual-resonance characteristic. At the optimal design point of 2.84 mm, two resonances are observed at approximately 12.8 GHz and 17.1 GHz. The lower resonance is primarily associated with the coaxial-to-patch interface, while the higher resonance arises from the subsequent impedance transformation into the SICL. The 2.84 mm configuration represents the critical compensation state where the parasitic inductance of the vertical pin is neutralized by the patch's capacitive loading. This specific diameter ensures that the separation of the two resonances is sufficient to cover the desired bandwidth with a deep matching level of less than −20 dB. The sensitivity analysis reveals that decreasing the diameter below this optimum reduces the capacitive compensation, causing both resonances to shift toward higher frequencies and resulting in a low return loss due to an under-compensated inductive junction. Conversely, increasing the diameter beyond the optimal value introduces excessive parasitic capacitance, shifting the resonances to lower frequencies and degrading the matching in the center of the Ku-band, as evidenced by the rise in S_{11} toward −18 dB. Consequently, the circular patch acts as a vital fine-tuning mechanism that precisely aligns the resonant modes to achieve a maximally flat, wideband response.

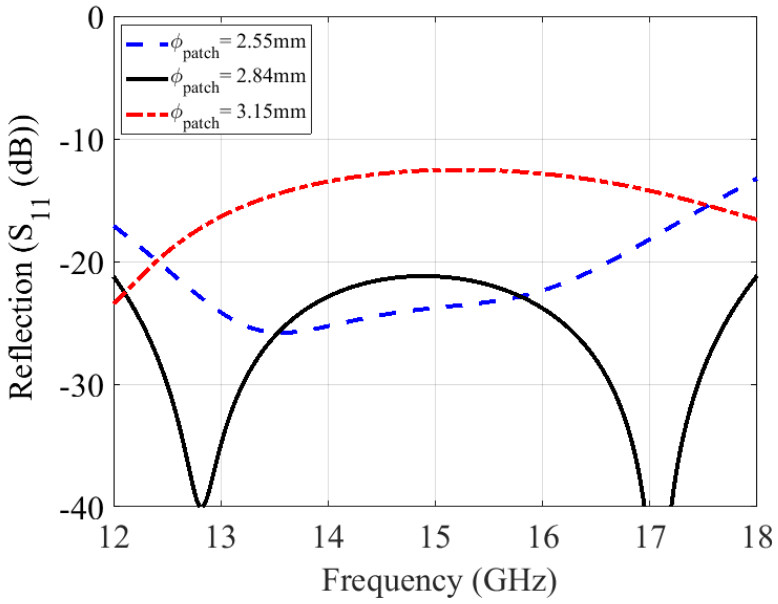

Figure 5. Parametric study of the circular patch diameter ϕ_{patch} on the transition performance.

Following the circular patch, a matching transformer with a width W_t and a length l_t is integrated into the design. This transformer enhances the transition's ability to smoothly couple the coaxial line's impedance to the SICL. The presented design not only extends the operational bandwidth but also mitigates the sensitivity to fabrication tolerances observed in traditional direct transition methods. By providing additional degrees of freedom in matching the coaxial line to the SICL, the proposed configuration achieves a robust matching level of 20 dB, as demonstrated in Figure 6, where the optimum dimensions are listed in Table 1.

Table 1. The dimensions of the proposed transition in millimeter.

Parameter	w_f	w_g	w_t	l_t	l_s	h_1
Value	0.95	4.3	2.66	1.96	2.9	0.762
Parameter	h_2	ϕ_h	ϕ_v	ϕ_{pill}	ϕ_{patch}	p_v
Value	0.762	0.83	0.38	1.05	2.84	0.75

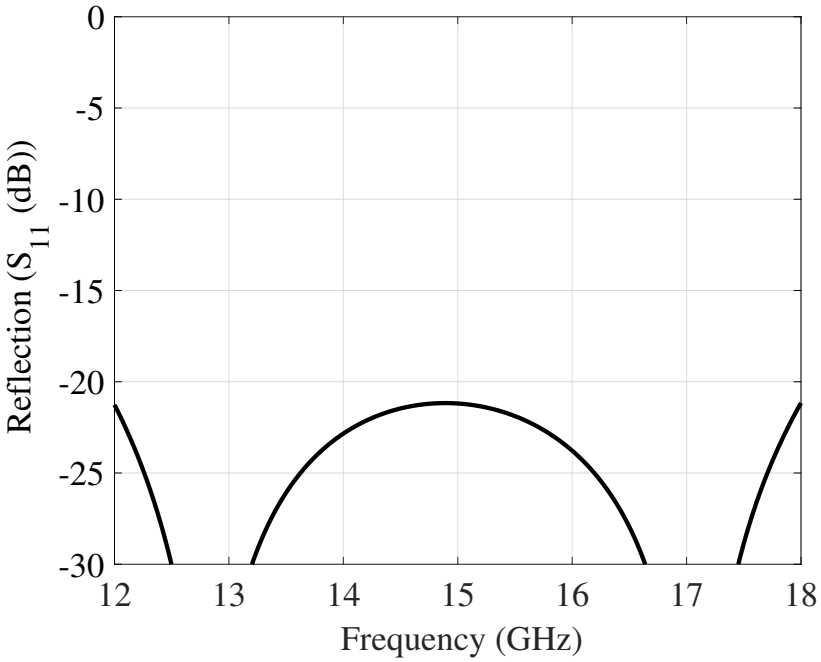

Figure 6. Simulated S_{11} of the proposed transition with optimum dimensions.

3. Results

The performance of the proposed transition was experimentally validated by fabricating and measuring a back-to-back configuration, as depicted in Figure 7. To assemble the fabricated transition layers, epoxy was used at high temperature and pressure [31]. The S-parameters were measured using the (N52271A) PNA network, and the comparison between the measured and simulated results is illustrated in Figure 7. Remarkably, there is a strong agreement between the measured and simulated S-parameters. The achieved results show a 40% relative bandwidth at 15 GHz, with a matching level of −15 dB and an insertion loss less than −0.6 dB.

The performance evaluation of the proposed transition involves a comparison with state-of-the-art SICL transition structures. Table 2 provides a comprehensive overview of these transition types. One such transition is a vertical SICL-coaxial configuration, achieving a matching level below −15 dB from 12 to 18 GHz [20]. However, the use of a metallic housing to accommodate the substrate results in a larger size, posing challenges for integration into compact designs. Another reported configuration involves a shielded suspended SICL with an SMA connector, achieving a matching level of −14 dB from 6 to 10 GHz [24]. This approach necessitates a metallic housing and meticulous soldering, introducing complexity and increasing manufacturing costs. Furthermore, a transition configuration utilizing two cascaded transmission lines connected to an orthogonal coaxial cable interface has been proposed [25]. However, this solution is lengthy and provides a matching level below −19 dB over a narrow bandwidth. In addition, a rectangular waveguide (RW) transition has been reported in [26], which uses a SICL-based approach for high-frequency applications. It operates

over a frequency range of 17.4 to 25 GHz in the K-band, but the return loss is relatively poor (around −10 dB) and the design suffers from relatively high insertion loss exceeding 1.2 dB/in per single transition. While the compact footprint allows integration into dense arrays, the high insertion loss limits its practical efficiency. Similarly, a broadband SICL-to-waveguide transition has been proposed in [27], achieving a wide simulated bandwidth from 20.23 to 32 GHz with a return loss better than 10 dB. However, this design is validated only through simulations and relies on a multilayer configuration with additional structural elements to enhance bandwidth. Moreover, the corresponding insertion loss is relatively high, reaching approximately 2.54 dB/in, which may limit its practical implementation in low-loss systems. Another broadband transition from conductor-backed coplanar waveguide with substrate-integrated coaxial line has been reported in [28], operating from 4.24 to 8.04 GHz, but the insertion loss is relatively high, more than 0.732 dB/in, limiting practical efficiency and compact integration. Another transition from grounded coplanar waveguide to substrate-integrated coaxial line has been reported in [29], operating from 24 to 30 GHz. Although the design provides good shielding with matching below −13 dB, the reported transmission loss corresponds to approximately 1.9 dB/in, which represents a relatively high propagation loss for compact millimeter-wave interconnects. In contrast, our proposed design offers a wide bandwidth transition covering the 12–18 GHz range with a deep matching level of −15 dB and low insertion loss using a K-connector. Compared to the transitions reported in the literature and summarized in Table 2, our design emerges as a promising candidate for wideband applications. It eliminates the need for a metallic housing, simplifies the manufacturing process, and achieves superior performance in terms of matching level and insertion loss.

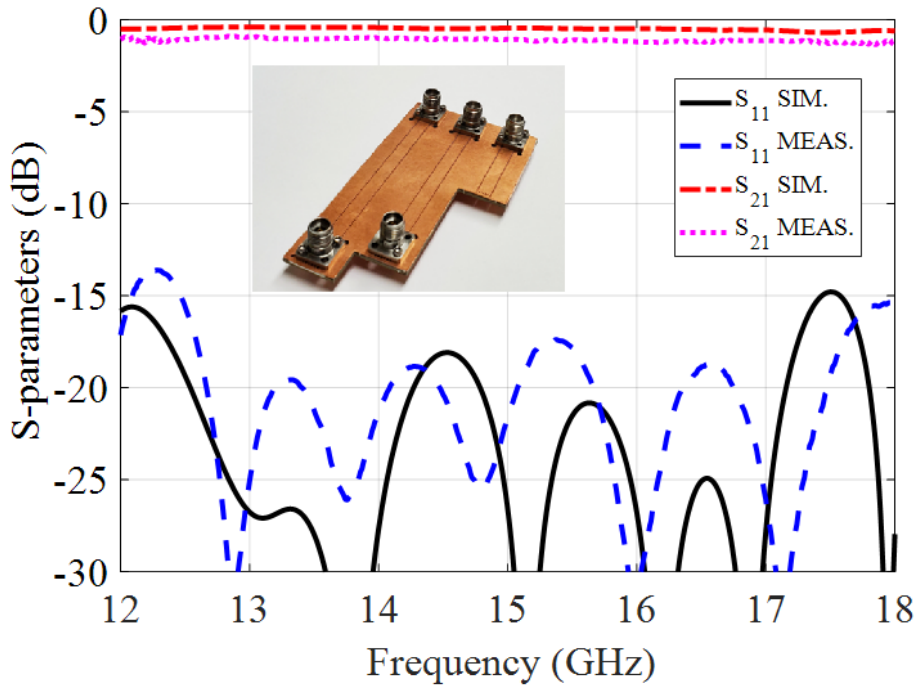

Figure 7. Fabricated and validation of the proposed prototype transition including back-to-back prototype and measured S-parameters.

Table 2. Comparison of state of the art SICL Transitions.

Ref.	Con.	Freq.	RL (dB)	IL (/in)	Housing
[20]	SMA	12–18 GHz	−15/B2B	N.A	Yes
[24]	SMA	6–10 GHz	−14/B2B	N.A	Yes
[25]	K	18–22 GHz	−19/Single	N.A	No
[26]	RW	17.4–25 GHz	−10 dB/single	1.2 dB	No
[27]	RW	20.2–32 GHz	−10/Single	1 dB	No
[28]	CPW	4.24–8.04 GHz	−12/Single	0.732 dB	No
[29]	GCPW	24–30 GHz	−13/Single	1.9 dB	No
Proposed Work	K	12–18 GHz	−15/B2B	0.2 dB	No

4. Conclusions

The article introduces a novel right-angle coax-to-SICL transition with outstanding electrical performance in a compact form factor. It effectively covers the full Ku-band with a deep matching level of more than 20 dB. Using an air-filled K-connector, optimal electrical characteristics and impedance matching have been achieved in a compact form up to 18 GHz. The fabricated transition has been tested in a back-to-back configuration, demonstrating excellent agreement between measured and simulated results, with a matching level of −15 dB and an insertion loss of −0.22 dB/inch across the entire bandwidth. This innovative design holds promise for high-frequency applications, paving the way for further advances.

Author Contributions: Conceptualization, S.I.S., M.E. and A.S.; methodology, M.M.M.A. and S.I.S.; software, M.M.M.A. and S.I.S.; validation, M.E., A.S. and G.G.; writing—original draft preparation, M.M.M.A. and S.I.S.; writing—review and editing, M.E., G.G. and A.S.; supervision, A.S.; funding acquisition, A.S. All authors have read and agreed to the published version of the manuscript.

Funding: This research received no external funding.

Institutional Review Board Statement: Not applicable.

Informed Consent Statement: Not applicable.

Data Availability Statement: The data that support the findings of this study are available from the corresponding author upon reasonable request.

Acknowledgments: The authors would like to acknowledge the support of Scientific Microwave Cooperation, and especially Gada Saad, for allowing us to perform the measurements and providing the connectors used in these experiments.

Conflicts of Interest: The authors declare no conflicts of interest.

References

1. Brito, J.M.C.; Mendes, L.L.; Gontijo, J.G.S. Brazil 6G project—An approach to build a national-wise framework for 6G networks. In *2nd 6G Wireless Summit (6G SUMMIT), Levi, Finland, March 2020*; IEEE: Piscataway, NJ, USA, 2020; pp. 1–5.
2. Chen, S.; Sun, S.; Kang, S. System integration of terrestrial mobile communication and satellite communication—the trends, challenges and key technologies in B5G and 6G. *China Commun.* **2020**, *17*, 156–171. [CrossRef]
3. Chen, S.; Zhang, J.; Jin, Y.; Ai, B. Wireless powered IoE for 6G: Massive access meets scalable cell-free massive MIMO. *China Commun.* **2020**, *17*, 92–109. [CrossRef]
4. Hong, W.; Zhou, J.; Chen, J.; Jiang, Z.; Yu, C.; Guo, C. Asymmetric full-digital beamforming mmWave massive MIMO systems for B5G/6G wireless communications. In *IEEE Asia-Pacific Microwave Conference (APMC), Hong Kong, China, December 2020*; IEEE: Piscataway, NJ, USA, 2020.
5. Karmokar, D.K.; Esselle, K.P.; Hay, S.G. Fixed-frequency beam steering of microstrip leaky-wave antennas using binary switches. *IEEE Trans. Antennas Propag.* **2016**, *64*, 2146–2154. [CrossRef]

6. Ali, M.M.M.; Shams, S.I.; Sebak, A.-R. Printed ridge gap waveguide 3-dB coupler: Analysis and design procedure. *IEEE Access* **2018**, *6*, 8501–8509. [CrossRef]
7. Ali, M.M.M.; Sebak, A. 2-D scanning magnetoelectric dipole antenna array fed by RGW Butler matrix. *IEEE Trans. Antennas Propag.* **2018**, *66*, 6313–6321. [CrossRef]
8. Chang, H.-C.; Li, R.-S.; Shih, T.-Y. Design of an 8 × 8 stripline Butler matrix with beam steering capability. In *IEEE Antennas and Propagation Society International Symposium, San Diego, CA, USA, July 2008*; IEEE: Piscataway, NJ, USA, 2008; pp. 1–4.
9. Wincza, K.; Gruszczynski, S.; Sachse, K. Design of integrated stripline multibeam antenna arrays fed by compact Butler matrices. In *IEEE Antennas and Propagation Society International Symposium, Honolulu, HI, USA, June 2007*; IEEE: Piscataway, NJ, USA, 2007.
10. Zhu, H.; Sun, H.; Jones, B.; Ding, C.; Guo, Y.J. Wideband dual-polarized multiple beam-forming antenna arrays. *IEEE Trans. Antennas Propag.* **2019**, *67*, 1590–1604. [CrossRef]
11. Gatti, F.; Bozzi, M.; Perregrini, L.; Wu, K.; Bosisio, R.G. A novel substrate integrated coaxial line (SICL) for wide-band applications. In *European Microwave Conference, Manchester, UK, 2006*; IEEE: Piscataway, NJ, USA, 2006; pp. 1614–1617.
12. Dai, X.; Li, A.; Luk, K.M. A wideband compact magnetoelectric dipole antenna fed by SICL for millimeter-wave applications. *IEEE Trans. Antennas Propag.* **2021**, *69*, 5278–5285. [CrossRef]
13. Ali, M.S.; Naveed, H.; Abbasi, M.A.B.; Shoaib, N.; Fusco, V.F. Substrate-integrated coaxial line (SICL) Rotman lens beamformer for 5G/B5G applications. *Electronics* **2023**, *12*, 69. [CrossRef]
14. Li, W.; Xu, J.; Zhao, R.; Hong, W. Compact broadband substrate-integrated coaxial line 2-D beamforming network and its multibeam array antenna applications. *IEEE Trans. Microwave Theory Tech.* **2024**, *72*, 262–274. [CrossRef]
15. Bulja, S.; Mirshekar-Syahkal, D.; Yazdanpanahi, M. Novel wide-band transition between finite ground coplanar waveguide and balanced stripline. In *European Microwave Integrated Circuits Conference (EuMIC), Rome, Italy, September 2009*; IEEE: Piscataway, NJ, USA, 2009; pp. 301–303.
16. Jankovic, U.; Basu, A.; Budimir, D. Planar transitions from substrate integrated coaxial line to single-layer transmission lines and waveguides. In *IEEE MTT-S International Microwave and RF Conference (IMaRC), Kolkata, India, 2018*; IEEE: Piscataway, NJ, USA, 2018; pp. 1–4.
17. Krishna, I.S.; Mukherjee, S. Design of wideband microstrip to SICL transition for millimeter-wave applications. *IEEE Access* **2020**, *8*, 4250–4254. [CrossRef]
18. Kumar, G.A.; Poddar, D.R. Broadband rectangular waveguide to suspended stripline transition using dendritic structure. *IEEE Microw. Wirel. Compon. Lett.* **2016**, *26*, 900–902.
19. Liu, Q.; Liu, Y.; Wu, Y.; Shen, J.-Y.; Li, S.; Yu, C.; Su, M. A substrate integrated waveguide to substrate integrated coaxial line transition. *Prog. Electromagn. Res. C* **2013**, *36*, 249–259. [CrossRef]
20. Shen, R.; Kong, D.; Sun, D. A design of stripline–coaxial vertical transition with ultra-broadband. In *International Conference on Microwave and Millimeter Wave Technology, Chengdu, China, May 2010*; IEEE: Piscataway, NJ, USA, 2010; pp. 1514–1517.
21. Krishna, I.S.; Mukherjee, S. A substrate integrated coaxial line dual-band balun for 5G applications. In *2018 Asia-Pacific Microwave Conference (APMC), Kyoto, Japan, 2018*; IEEE: Piscataway, NJ, USA, 2018; pp. 1190–1192.
22. Xia, L.; Xu, R. Broadband LTCC transition from coaxial connector to stripline for 60GHz application. In *International Conference on Computational Problem-Solving (ICCP), Leshan, China, October 2012*; IEEE: Piscataway, NJ, USA, 2012; pp. 52–54.
23. Krishna, I.S.; Mukherjee, S. Design of wideband coaxial-to-substrate integrated coaxial line (SICL) planar transition. In *2018 International Conference on Signal Processing and Communications (SPCOM), Bangalore, India, 2018*; IEEE: Piscataway, NJ, USA, 2018; pp. 152–156.
24. Inclan-Alonso, J.M.; Fernandez Gonzalez, J.-M.; Sierra-Perez, M. Low losses power distribution networks in stripline technology for planar array antennas. *Prog. Electromagn. Res.* **2013**, *143*, 369–384. [CrossRef]
25. Wang, Y.; Oliver, E.; Ness, J.; Abbosh, A. Orthogonal coaxial to suspended substrate transition for K band operation. In *2018 Australian Microwave Symposium (AMS), Brisbane, QLD, Australia, 2018*; IEEE: Piscataway, NJ, USA, 2018; pp. 13–14.
26. Wei, Y.; Arnold, C.; Hong, J. A K/Ka-Band Reconfigurable Substrate Integrated Coaxial Line to Waveguide Transition. *IEEE Access* **2022**, *10*, 65037–65043. [CrossRef]
27. Liao, Q.; Chen, C.; Ji, Y.; Hou, Z.; Wang, S.; Wu, W. A Broadband and Compact SICL to Waveguide Transition. In *2022 IEEE MTT-S International Microwave Workshop Series on Advanced Materials and Processes for RF and THz Applications (IMWS-AMP)*; IEEE: Piscataway, NJ, USA, 2022; pp. 1–3.
28. Nayak, A.K.; Filanovsky, I.M.; Moez, K.; Patnaik, A. Broadband Conductor Backed-CPW With Substrate-Integrated Coaxial Line to SIW Transition for C-Band. *IEEE Trans. Circuits Syst. II Express Briefs* **2022**, *69*, 2428–2432. [CrossRef]
29. Van Messem, L.; Moerman, A.; Caytan, O.; Rogier, H.; Lemey, S. Substrate Integrated Coaxial Line Millimeterwave Components Manufactured in Standard PCB. In *2023 IEEE 32nd Conference on Electrical Performance of Electronic Packaging and Systems (EPEPS)*; IEEE: Piscataway, NJ, USA, 2023; pp. 1–3.

30. *CST Studio Suite 2025*; Dassault Systèmes: Vélizy-Villacoublay, France, 2025.
31. Veldhuijzen van Zanten, J.; Gorter, A.; van Driel, W.D.; Zhang, G.Q. Method to determine thermoelastic material properties of constituent and copper-patterned layers of multilayer printed circuit boards. *J. Mater. Sci. Mater. Electron.* **2018**, *29*, 4900–4914. [CrossRef]